Hindawi
Shock and Vibration
Volume 2019, Article ID 7297392, 16 pages
https://doi.org/10.1155/2019/7297392

*Research Article*

# Research on Vibration Reduction Design of Foundation with Entangled Metallic Wire Material under High Temperature

**Yue Zhu, Yiwan Wu, Hongbai Bai, Zheyu Ding, and Yichuan Shao**

*Engineering Research Center for Metal Rubber, Fuzhou University, Fuzhou 350116, Fujian, China*

Correspondence should be addressed to Yiwan Wu; wuyiwan@fzu.edu.cn

Received 28 May 2019; Accepted 4 August 2019; Published 18 September 2019

Academic Editor: Jussi Sopanen



When the submarine is sailing at full speed, the power cabin has an abnormally high temperature. However, in the previous research on the vibration reduction design of the foundation, the influence of high temperature on the vibration characteristics of the foundation is not taken into account. In this paper, a new composite foundation with entangled metallic wire material (EMWM) is presented to reduce the vibration of the foundation. The energy transfer path of the foundation was obtained by the power flow method, and then the layout of EMWM was determined. The optimization of the constraining layer was carried out by modal analysis. The damping performance of the composite foundation with EMWM was validated by the thermal-vibration joint test. The results show that, at room temperature, the composite foundation has remarkable vibration reduction efficiency in the middle and high-frequency bands. The maximum insertion loss can reach 15.37 dB. The insertion loss varies with the location of the excitation point. As the temperature rises to 300°C, the insertion loss in the low-frequency band was improved, and the insertion loss is not influenced by the excitation position.

## 1. Introduction

In modern warfare, the acoustic stealth performance of submarines directly affects their survival and attack. The prime sources of underwater noise for submarines are fluid noise, machinery noise, and structural borne noise [1]. The machinery noise mainly comes from various mechanical devices, weapons, and electrical equipment installed on submarines. The mechanical vibration and noise generated by these devices are transmitted to the hull structure through the support system (such as the foundation). And then, those vibration and sound are radiated to the water.

The foundation is a key link of the vibration transmission path. The vibration characteristic of the foundation is related to the acoustic stealth performance of submarines. The foundation is usually designed as an elastic support structure with damping function. However, some equipment and structures connected to the power machine often have more stringent alignment requirements, such as the installation of tail shaft and gear box. In this case, the foundation is designed to be rigid. Thus, flexible vibration isolation technology cannot be used to reduce the vibration of rigid foundation. To solve this problem, there are three methods to reduce the vibration of rigid foundation: adding blocking masses, using composite foundation, and laying viscoelastic damping material [2]. Researchers have done an enormous amount of research on these three methods.

The foundation is composed of several plates, and the blocking masses are often added to the plates for reflecting or suppressing vibration wave at specific wavelengths. Shi et al. [3] studied the influence of the blocking masses on the T-structure, which is commonly used in the foundation. The results show that the blocking masses can improve the structural vibration damping performance by over 5 dB. Che and Chen [4, 5] discussed the vibration energy transfer of two plates connected at any angle and analyzed the influence of the vibration resistance on the corners of two plates. Xia and Chen [6] studied the application of the blocking masses composed of viscoelastic sandwich composite on the cylindrical shell-side pallet. Yao et al. [7] conducted a full-band numerical analysis of the power cabin with a foundation

made of blocking masses by the use of the acoustic-solid coupling method and statistical energy method.

Composite foundation made of new materials, such as carbon fiber-reinforced composite materials, has better damping performance. Zhang et al. [8, 9] adopted a honeycomb structure to design a composite foundation that combines low-frequency vibration isolation and anti-shock. They also studied the influence of the number of honeycomb layers and cell wall thickness on the characteristic of the composite foundation. Wu et al. [10, 11] designed a marine foundation made of star-shaped porous materials and applied it to real ships. The results show that the vibration isolation performance of the new foundation is better than that of the traditional foundation. By the use of topology optimization method, Qing et al. [12, 13] obtained the optimal negative Poisson's ratio structure of functional units and designed a negative Poisson's ratio foundation with better low-frequency vibration damping performance and bearing capacity. Damping material is used for vibration damping without changing the original structure of the ship. The viscoelastic damping material can convert and dissipate vibrational energy when subjected to dynamic stresses and strains. In addition, the damping material has an effect in a wide frequency band. Liu et al. [14] designed a damping equipment foundation. It combines the damping material with the blocking masses. Garrison et al. [15] studied the effect of the coverage area, thickness, and position of the damping layer on the vibration characteristics of the plate. The results show that the strip-shaped constrained damping is arranged off-center along the length direction, which produces an optimal effect in a wide frequency band.

The core material and the panel with strong energy absorbing performance can form a sandwich structure, which has broad application prospects in ship vibration reduction. Compared with free damping, the constrained damping produces a larger shear strain under harmonic excitation, resulting in more energy dissipation. The current research mostly focuses on the dynamic performance of the sandwich panel. Merideno et al. [16] studied the parameters of the sandwich confinement damper and analyzed the properties of viscoelastic materials. The properties of the viscoelastic material, the geometrical parameter design of the metal plate and the viscoelastic layer, and the influence of different sequences on the damper design were analyzed. D'Alessandro et al. [17] summarized the research on the acoustic performance of sandwich panels. Wang and Ma [18] combined wave analysis with finite element method to explore the acoustic transmission characteristics in lattice sandwich panels. Lou et al. [19] studied the free vibration problems of lattice sandwich beams under several typical boundary conditions. Yang et al. [20] analyzed the vibration and damping properties of hybrid carbon fiber composite pyramid truss sandwich panels. Assaf and Guerich [21] proposed that the strain and kinetic energies of the sandwich plates are written in terms of the mean and relative in-plane displacements of the faces and the transverse deflection of the plate.

The vibration reduction design of foundation under high temperature is still a difficult technical problem. Traditional polymer materials such as rubber will accelerate aging with the rise of temperature. When the temperature is too high, the damping material may even crack and carbonize, which will greatly reduce its service life. A variety of new damping materials have emerged, and the most representative of which is entangled metallic wire material (EMWM) [22–27]. EMWM is a new type of damping materials formed by spiraling, stretching, winding, and stamping of metal wires. Due to the metal characteristics of the EMWM, it has high temperature resistance. This makes EMWM a new way to solve the vibration damping problem in harsh environments such as high temperature [28]. Hou et al. [29] studied the damping properties of disc-shaped EMWM in high- and low-temperature environments. The results show that the damper has a good and stable damping performance in the temperature range of −70°C to 300°C.

To reduce the vibration of the foundation under high temperature, a composite foundation with entangled metallic wire material is proposed. A power flow calculation is performed to determine the position for laying EMWM. A modal analysis of the foundation is conducted for optimizing the constraining layer. Finally, a thermal-vibration joint test for foundation is conducted to validate the proposed method.

## 2. EMWM Insertion Damping Structure

*2.1. Entangled Metallic Wire Material.* Entangle metallic wire material is a metallic damping material. In this paper, the EMWM layer is made of 304 (06Cr19Ni10) stainless steel wires. The preparation of the EMWM is referring to [28]. To prepare the plate-like EMWM with holes, the rough porous base material was penetrated by hole making shaft, and then the molding process is carried out. Taking the preparation of medium-sized EMWM as an example, the preparation schematic and the rough porous base material of EMWM are shown in Figure 1. EMWM of different sizes can be prepared by adding or subtracting filling blocks.

The EMWM specimens are shown in Figure 2, and the forming parameters are shown in Table 1.

*2.2. Insertion Damping Structure.* As shown in Figure 3, to reduce the vibration of the baseplate (foundation), an EMWM insertion damping structure is presented. Under high temperature, the constraining layer and EMWM cannot be fixed to the baseplate by conventional adhesive. In this paper, the constraining layer and the EWMW layer are fixed to the foundation by screw connection.

When the baseplate is excited, the baseplate will produces a displacement response, and the constraining layer will also produces a displacement response. The deviation in the displacement between baseplate and constraining layer will cause the EMWM layer to produce tension-compression deformation. When the entangled metallic wire material is deformed in micron scale, the internal metal wire will slip and lead to energy dissipation [30]. Therefore, the energy dissipation mechanism of the insertion damping structure is extrusion friction energy dissipation.

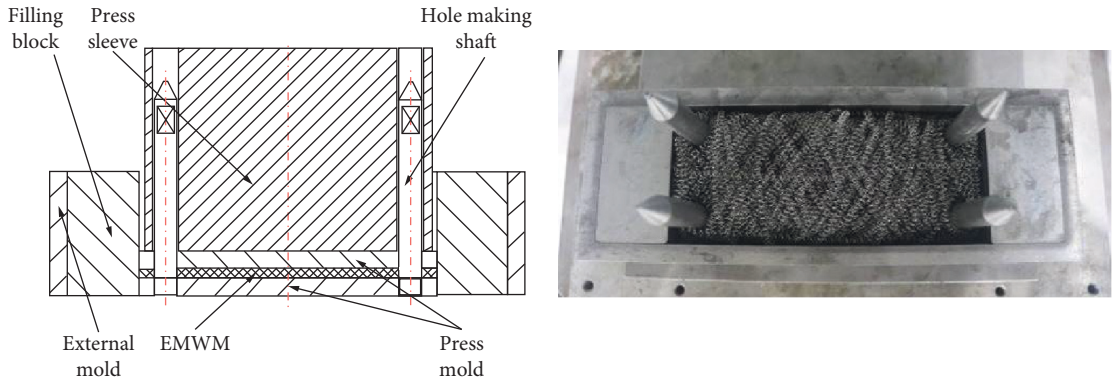


Figure 1: Mold and rough porous base material of EMWM. (a) Schematic diagram of the pressing mold. (b) Rough porous base material of EMWM.

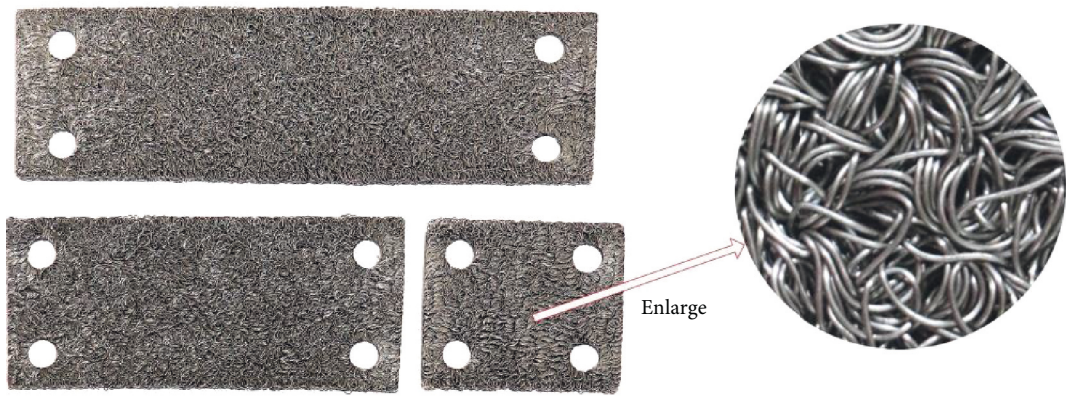


Figure 2: EMWM specimens.

Table 1: Formation parameters.

| EMWM type | S | M | L |
|---|---|---|---|
| Dimension (mm) | $84 \times 74 \times 4$ | $168.5 \times 74 \times 4$ | $249 \times 74 \times 4$ |
| Density (g/cm$^3$) | 2.595 | 2.596 | 2.584 |
| Forming pressure (kN) | 1260 | 1890 | 2394 |

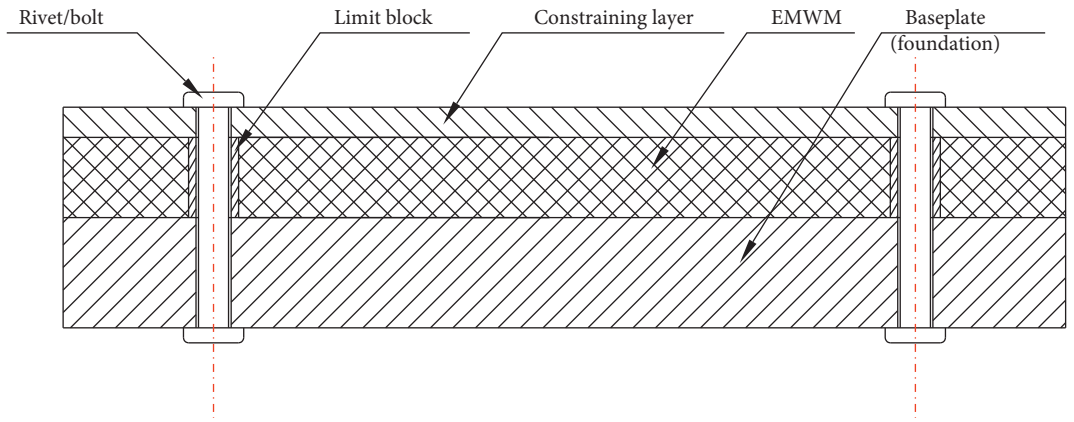


Figure 3: Two-dimensional schematic diagram of the EMWM insertion damping structure.

## 3. EMWM Composite Foundation

*3.1. Initial Structure of the Steel Foundation.* A simplified foundation is used as the research subject, and its dimensions are shown in Figure 4 and Table 2. The foundation is composed of a face plate, connection plates, web plates, and brackets. A fixed plate is used to represent the hull. To improve the stiffness of the fixed plate, the bottom of the fixed plate is welded with three horizontal and two longitudinal ribs. The foundation is fixed to the fixed plate by welding. The fixed plate is supported by four supports.

The foundation and the fixed plate are made of 45 steel (C45E4). The material properties of 45 steel are as follows: density is 7890 kg/m$^3$, Poisson's ratio is 0.3, and loss factor is 0.002. Young's modulus and thermal expansion coefficient of 45 steel are affected by the ambient temperature, as shown in Table 3.

*3.2. Position Analysis for Laying EMWM.* The lightweight of ships or submarines is an important technical specification, which should be considered in the design of composite foundation. Power flow can reflect the relationship between the magnitude and phase of force and velocity vector. It means that it can describe the vibration more comprehensively. Therefore, the power flow is selected as an evaluation index to reflect structural vibration [31, 32].

The foundation is mainly composed of several flat-plate structures. When a flat-plate structure is excited by a single-frequency steady-state force, in consideration of the thickness of the plate, the power flow per unit width $pf$ can be expressed as follows:

$$pf_x = -\frac{\omega}{2}\mathrm{Im}\left[N_x\tilde{u}_0^* + N_{xy}\tilde{v}_0^* + Q_x\tilde{\omega}_0^* + M_x\tilde{\theta}_y^* - M_{xy}\tilde{\theta}_x^*\right], \tag{1}$$

$$pf_y = -\frac{\omega}{2}\mathrm{Im}\left[N_y\tilde{v}_0^* + N_{yx}\tilde{u}_0^* + Q_y\tilde{\omega}_0^* - M_y\tilde{\theta}_x^* + M_{yx}\tilde{\theta}_y^*\right], \tag{2}$$

where $N_x$, $N_y$, and $N_{xy} = N_{yx}$ are complex membrane forces per unit width; $Q_x$ and $Q_y$ are the complex shear forces per unit width; $M_x$, $M_y$, and $M_{xy} = M_{yx}$ are the complex internal moments per unit width; $\tilde{u}_0^*$, $\tilde{v}_0^*$, and $\tilde{\omega}_0^*$ are the complex conjugate of translational displacements; $\tilde{\theta}_x^*$, $\tilde{\theta}_y^*$, and $\tilde{\theta}_z^*$ are the complex conjugates of rotational displacement; $\omega$ is the excitation frequency; and Im denotes an imaginary part. The positive orientations of internal forces and displacements used to formulate structural intensity in equations (1) and (2) are shown in Figure 5.

In this paper, the laying position of EMWM is determined by the power flow distribution of the foundation.

The first-order natural frequency of the foundation is larger than that of the fixed plate. To avoid the influence of the fixed plate, the vibration of the foundation is analyzed separately. The boundary condition of the foundation is set as clamped. The excitation points are located at the center and the corner of the face plate, respectively. The finite element model, excitation points, and boundary conditions are shown in Figure 6.

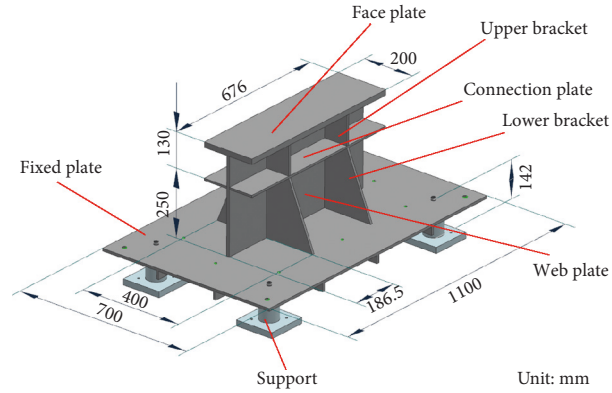


Figure 4: Structural parameters of steel foundation.

Table 2: Thickness of each plate of the foundation.

| Name | Thickness (mm) |
|---|---|
| Face plate | 20 |
| Web plate | 12 |
| Bracket | 9 |
| Connection plate | 8 |

Table 3: Thermophysical properties of 45 steel.

| Temperature (°C) | 20 | 300 |
|---|---|---|
| $E$ (GPa) | 210 | 196 |
| $\alpha$ ($10^{-6}$)/°C | 11.59 | 13.09 |

The modal response and power flow of the foundation are solved by direct method with the commercial software "ABAQUS." The sweep frequency is set to 10 Hz–500 Hz. The sweep rate is 1 oct/min. A unit excitation is applied at points A and B, respectively. The thermal expansion force will replace the excitation force at high temperature, and thus the power flow of the foundation is solved only at room temperature (20°C). Taking the second-order natural frequency as an example, the results of the calculation are shown in cloud and vector diagram, as shown in Figure 7.

As shown in Figure 7(a), it can be seen that the distribution of power flow is mainly concentrated in the middle of the face plate, the edge of the brackets, and the upper portion of the web plates. And there is also a partial power flow vector distribution on the connection plates. It can be seen from Figure 7(b) that the power flow is concentrated on one side of the face plate, the edge of the brackets, the top of the web plates, and the connecting plates. The larger the power flow means the higher the vibration energy, and thus the EMWM should be laid on the corresponding place. The upper part of the face plate needs to be placed with equipment, and thus the face plate is single-sided covered with EMWM. The other parts are covered with EMWM on both sides. Therefore, entangled metallic wire material (EMWM) should be laid on following places: ① the lower surface of the upper face plate, ② the connection plate,

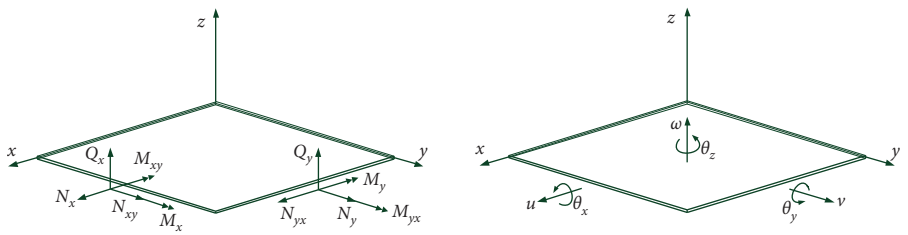


Figure 5: Internal force and displacement of the flat unit.

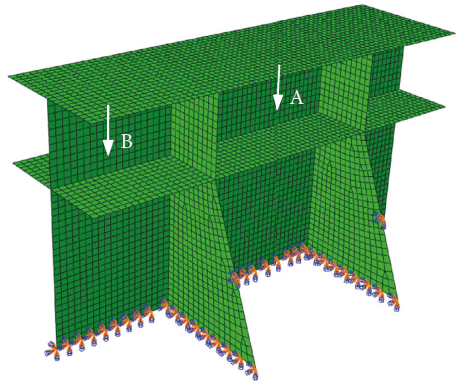


Figure 6: The finite element model, excitation points, and boundary conditions.

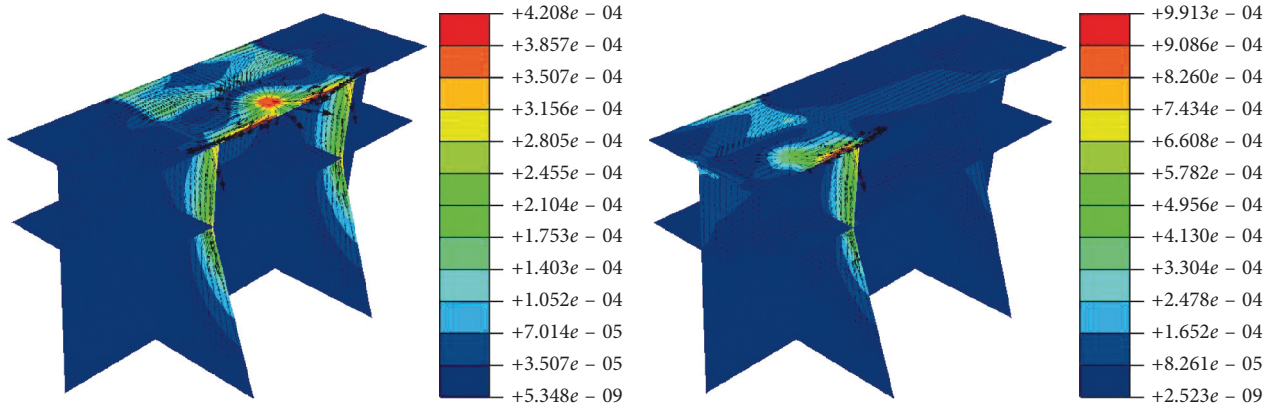


Figure 7: Power flow cloud and vector diagram of foundation at room temperature. The incentive is located at (a) point A and (b) point B (unit: watt).

③ the upper part of web plate, ④ the upper bracket, and ⑤ bevelled portion of the lower bracket. As shown in Figure 8, to improve the damping performance of EWMW, the EWMW is used as the insertion damping layer.

As shown in Figure 9, the EMWM is made of space-structured wire. It is difficult to establish accurate finite element model of the EMWM. Therefore, no EMWMs are added in the simulation, and only the space between foundation and constraining layer under different modes is taken into account. The foundation and constraining layer are positioned by limit blocks. The structural diagram is shown in the cross-sectional view of Figure 8.

*3.3. Optimization of Constraining Layer.* The energy dissipation of the EMWM insertion damping structure is determined by the deformation of the EMWM layer. The EMWM was constrained by the foundation and constraining layers. The displacement deviation between the foundations and constraining layers will cause the EMWM layer to produce tension-compression deformation. The greater the displacement deviation, the more energy is dissipated by the EMWM. Therefore, to maximize the energy dissipation, the arrangement of bolts and the thickness of the constraining layer should be optimized to maximize the displacement deviation.

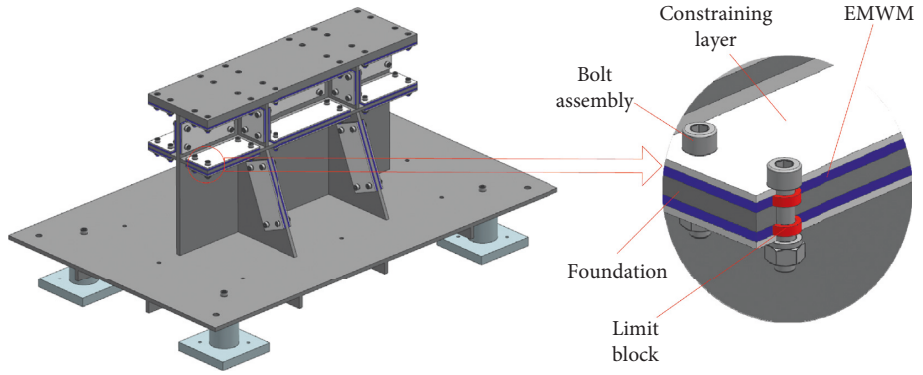


Figure 8: Arrangement scheme of the composite foundation.

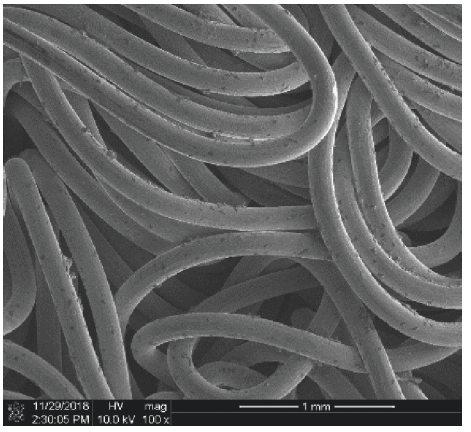


Figure 9: SEM image of the EMWM (100x enlargement).

Table 4: Installation methods of bolts.

| | Installation method |
|---|---|
| BA1 | Four bolts, fixed at four corners |
| BA2 | Two bolts, diagonally fixed at positions 2 and 4 |

Considering the location and the thickness of the EMWM layer, the thickness of the constraining layer is limited to 2~7 mm, and two bolt fixing methods are compared, as shown in Table 4. Since the foundation is a symmetrical structure, only the nonrepetitive part of the foundation is analyzed. To reduce the difficulty of analysis, when analyzing the influence of the insertion damping structure at one place, the insertion damping structures in other parts are removed and the corresponding excess holes are filled. The finite element mesh of the foundation at each position is presented in Figure 10.

The modal analysis of the foundation is conducted by the use of ABAQUS. The optimization method is as follows:

$$\begin{aligned}
&\text{Find:} \quad H_{\text{bf}}, H_{\text{br}}, H_{\text{wf}}, H_{\text{wr}}, H_{\text{cf}}, H_{\text{cr}}, H_{\text{fr}} = [h_1, h_2, h_3, \cdots, h_i, \cdots, h_n]^{\text{T}},\\
&\qquad\quad \text{BA} = [1, 2]^{\text{T}},\\
&\text{Max:} \quad D_{\text{bf}}, D_{\text{br}}, D_{\text{wf}}, D_{\text{wr}}, D_{\text{cf}}, D_{\text{cr}}, D_{\text{fr}} = \frac{1}{m}\sum_{j=1}^{m}\left|d_{\text{b},j} - d_{(\text{bf,br,wf,wr,cf,cr,fr}),j}\right|, \qquad (3)\\
&\text{s.t.} \quad h^{\text{b}} \le h_i \le h^{\text{t}}\\
&\qquad\quad f^{\text{b}} \le f_i \le f^{\text{t}},
\end{aligned}$$

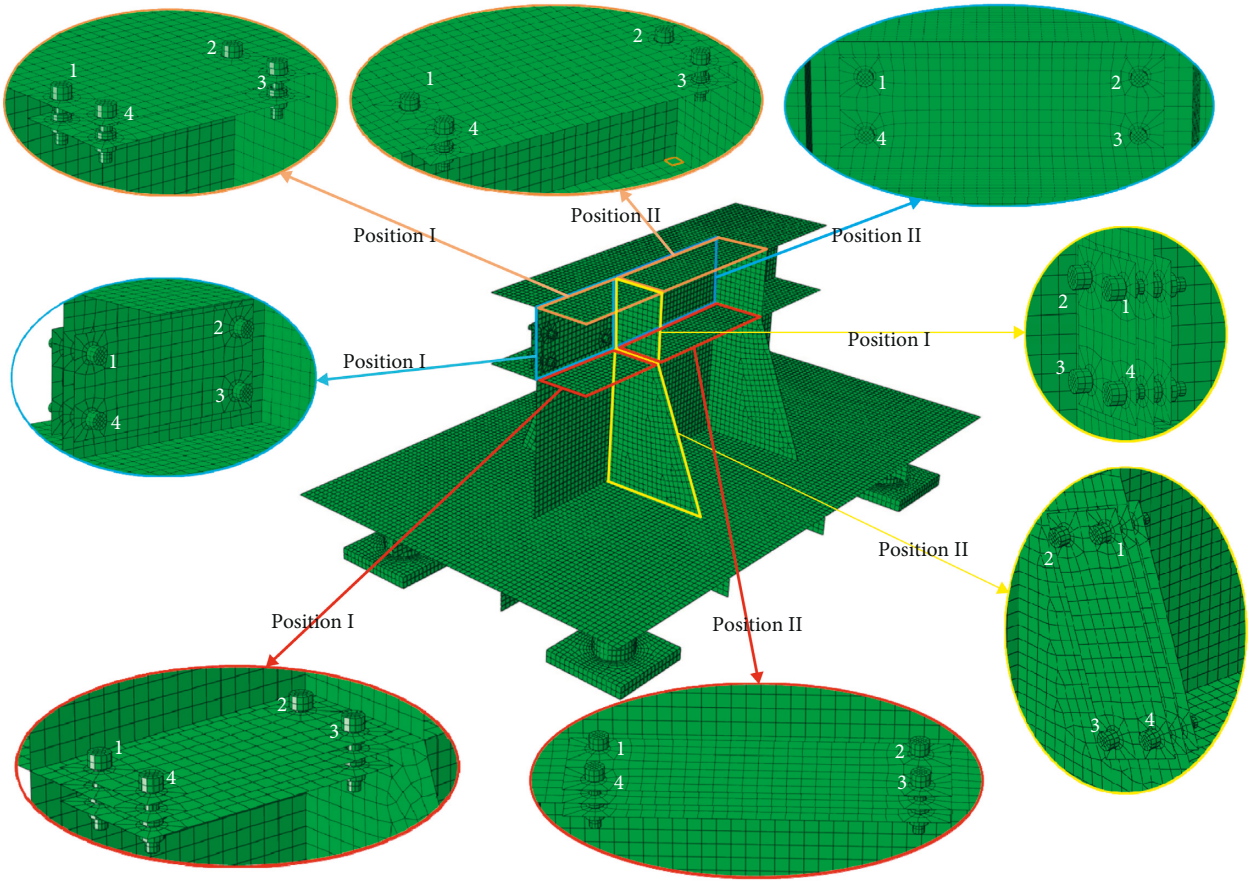


Figure 10: FEM model of each laying position.

where $H_{bf}$, $H_{br}$, $H_{wf}$, $H_{wr}$, $H_{cf}$, and $H_{cr}$ are the thickness of the upper and lower constraining layers at the corresponding positions of the brackets, the web plates, and the connection plates, respectively; $H_{fr}$ is the thickness of the lower constraining layers at the corresponding positions of the face plate; BA is the installation method of bolts; $d_{b,j}$ is the displacement component of the foundation in the normal direction of the foundation; $D_{bf}$, $D_{br}$, $D_{wf}$, $D_{wr}$, $D_{cf}$, and $D_{cr}$ are the displacement deviation between the foundation at the bracket, the web plate, the connection plate, and the corresponding upper and lower constraining layers; $D_{fr}$ is the displacement deviation between the foundation at the face plate and the corresponding lower constraining layer; $d_{(bf,br,wf,wr,cf,cr,fr),j}$ is the displacement component of the upper and lower constraining layers corresponding to the foundation of each position extending in the normal direction of the foundation, in which the face plate has only the lower constraining layer; $m$ is the number of mesh nodes of the foundation at each position, and it is also equal to the number of mesh nodes of the corresponding constraining layers; $h^b$ and $h^t$ are the upper and lower bounds of the thickness design variable, respectively; and $f^b$ and $f^t$ are the upper and lower limits of the analysis frequency interval, respectively. The upper constraining layer is near the head of the bolt, and the lower constraining layer is near the nut.

The boundary condition is set to be fixed at the bottom of the supports, and the temperature is 300°C. The displacement deviation between each position of the foundation and the corresponding constraining layer at the first three natural frequencies is obtained by modal calculation, as shown in Figures 11–14.

It can be seen from Figure 11 that, with the increase of the thickness of the constraining layer, $D_{fr}$ decreases in the first and second modes. In the third mode, with the increase of the thickness of the constraining layer, $D_{fr}$ at Position I decreases rapidly and then increases gradually. This trend of the quadrangular fixed method (BA1) is more obvious than that of the diagonal fixed method (BA2). Compared with BA2, BA1 increases the local stiffness, which reduces $D_{fr}$. However, when there is a large local change in the torsional mode, the change of $D_{fr}$ is more obvious with the changes of the thickness of the constraining layer.

In Figure 12, the change trends of $D_{bf}$ and $D_{br}$ of bracket position in the first two modes are different from the rest. The curves of $D_{bf}$ and $D_{br}$ show an upward trend. The average values of $D_{bf}$ and $D_{br}$ at Position I are smaller than the rest of the same order. The normal direction of the constraining layer is not in the same direction as the first two modes, which leads a small deformation of the constraining layer. Position I is located in the middle of the face plate and the connection plate. Therefore, the local stiffness is large, which weakens the degree of deformation. The bracket Positions I and II are different in the third-order mode. $D_{bf}$ and $D_{br}$ at Position I increase with the increase of the

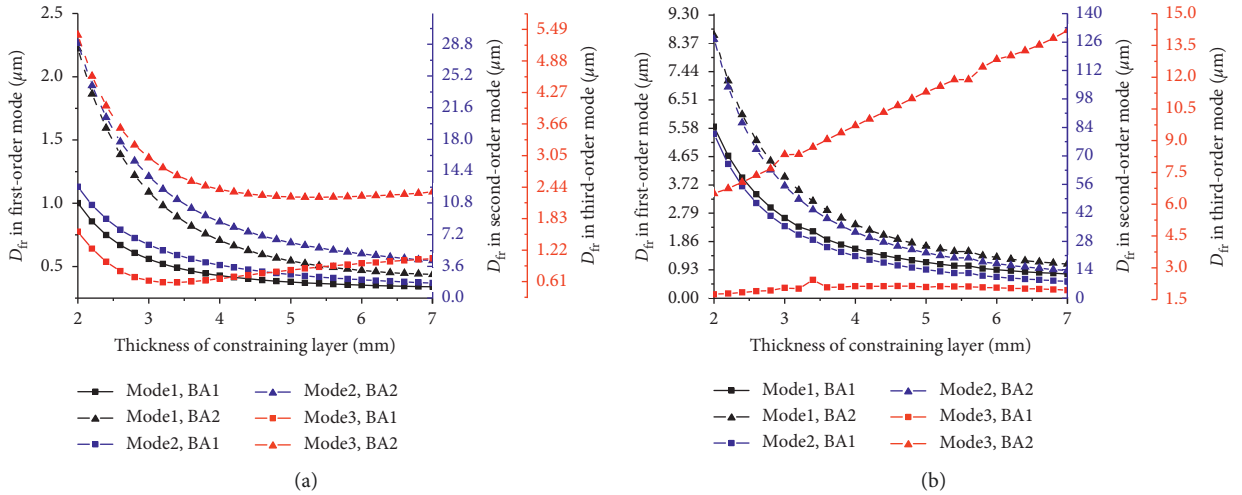


FIGURE 11: Displacement deviation between foundation and constraining layers in the position of the face plate. (a) Position I, lower constraining layer. (b) Position II, lower constraining layer.

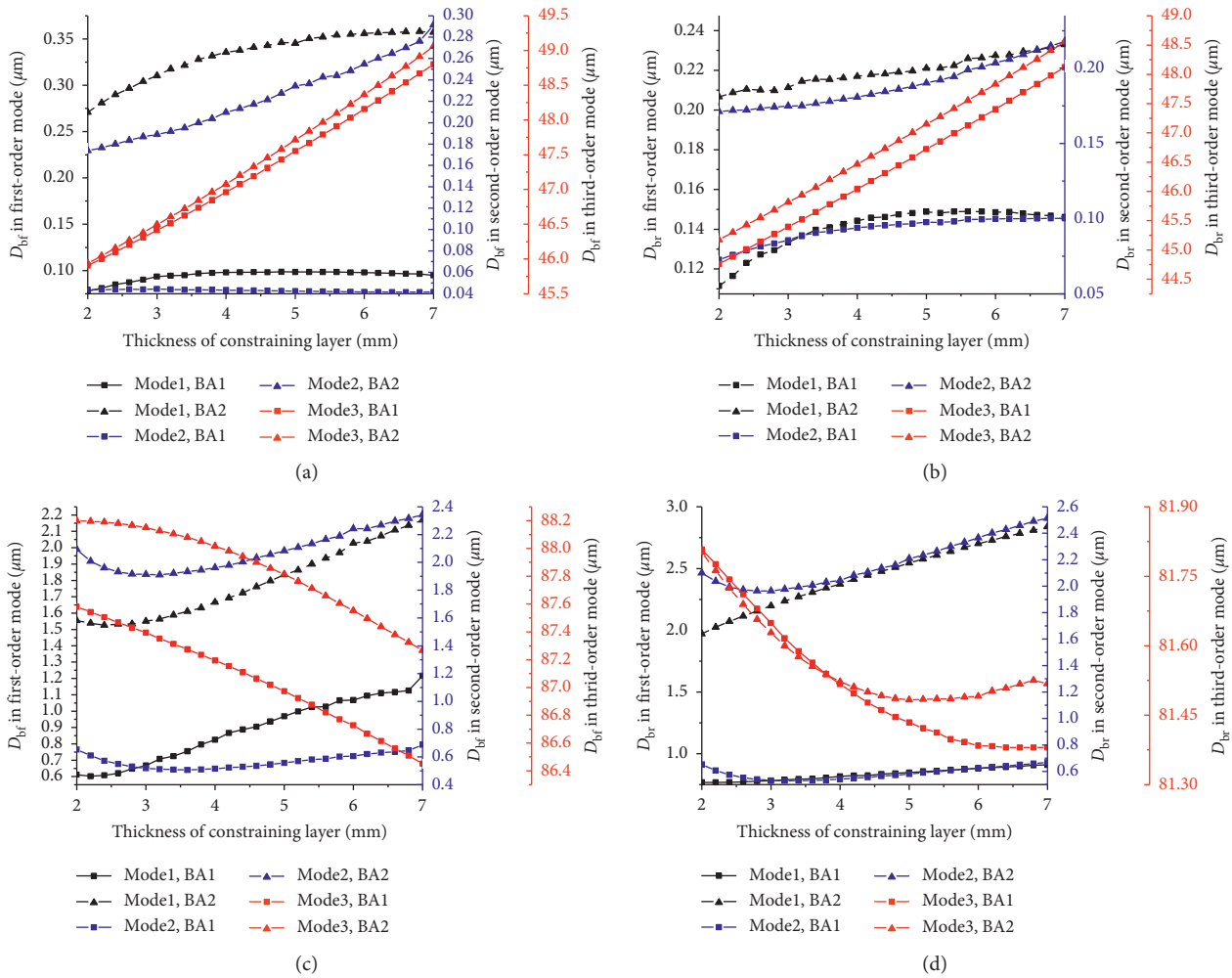


FIGURE 12: Displacement deviation between foundation and constraining layers in the position of the bracket. (a) Position I, upper constraining layer. (b) Position I, lower constraining layer. (c) Position II, upper constraining layer. (d) Position II, lower constraining layer.

thickness of the constraining layer. However, at Position II, $D_{bf}$ and $D_{br}$ show a significant downward trend. The reason is that the third-order mode torsion has a greater influence on Position I. The influence of the change of the foundation on the torsion is greater than that of the change of the constraining layer. Moreover, the thickness of the bracket is small. Thus, the deformation can offset the weakening effect caused by the increase of the local stiffness. Therefore, $D_{bf}$ and $D_{br}$ increase with the thickness of the constraining layer. The deformation at Position II is small, and it is difficult to offset the increase in local stiffness caused by the increase in the thickness of the constraining layer.

The first two modes of the foundation are forward-backward bending mode and up-down translational mode, respectively. Therefore, for the area of the foundation other than the bracket, when the thickness of the constraining layer increases, the bending mode should make the constraining layer form a larger displacement deviation between constraining layer and foundation due to the difference between the inside and outside. But, as the thickness of the constraining layer increases, the stiffness of the part, where the constraining layer is located, will increase at the same time. Thus, as shown in Figures 11, 13, and 14, the degree of bending deformation is weakened, and the actual displacement deviation between constraining layer and foundation decreases with the increase of the thickness of the constraining layer.

As can be seen from Figures 11–14, the displacement deviation between constraining layer and foundation of BA2 is larger than that of BA1.

The curves of $D_{fr}$ at Position I in the first three modes show a downward trend. Thus, the thinnest constraining layer is selected. The curves of $D_{fr}$ at Position II in the first two modes also show a downward trend. The trend of the curves in the third-order mode is different from that in the other modes. However, the corresponding value of the curve in the third-order mode is smaller than that in the other modes. Thus, the thinnest constraining layer is selected.

The curves of $D_{bf}$ and $D_{br}$ at Position I show an upward trend in the first three modes. Therefore, the thickest constraining layer is selected. However, in the first and third modes, the curves of $D_{bf}$ and $D_{br}$ at Position II show an upward trend, and the corresponding value of it is small. Its degree of upward trend is slightly smaller than the downward trend of it in the third mode. At the same time, increasing the thickness of the constraining layer is beneficial to $D_{bf}$ and $D_{br}$ in the first three modes. Considering the lightweight of the constraining layer, the thinnest constraining layer is selected.

In the first and third modes, the curves of the displacement deviation between constraining layer and foundation at two positions of the web plate show a downward trend. However, they show an upward trend in the second mode, the corresponding value of the curve is smaller than that in the other modes. Thus, the thinnest constraining layer of the web plate is selected.

The curves of the displacement deviation between constraining layer and foundation at two positions of the connection plate show a downward trend in the first three modes. Therefore, the thickest constraining layer is selected.

In summary, the final thickness of the constraining layers is shown in Table 5 and is unified in the diagonal fixing mode 2 to participate in the thermal-vibration joint test.

As can be seen from Figures 11–14, the above selected result makes the displacement deviation between constraining layer and foundation at each position in the first three-order mode produce micron-scale changes. Therefore, the insertion damping structure at all positions will dissipate the vibration energy [30].

## 4. Modal Verification

In this section, the modal simulation results will be validated by experimental modal analysis. Young's modulus of 45 steel will change under different temperatures. However, the difference between the modal analysis results at high temperature and those at room temperature is small. Thus, the modal validation of the steel foundation is carried out only at room temperature.

As shown in Figure 15, the steel foundation is placed on the rough ground. Because the external exciting force is much smaller than the friction force between the foundation and the ground, the boundary condition of the foundation can be regarded as the clamped boundary condition. The vibration exciter is suspended by elastic ropes. The vibration exciter sends sine sweep force (10–500 Hz, 80 N) to continuously excite the foundation. The response of the foundation is detected by four acceleration sensors to obtain the natural frequencies of the foundation. The excitation and response signals are recorded and processed by the use of the signal source and data acquisition submodule in real time. In general, it is enough to get the natural frequencies of the foundation by one acceleration sensor. However, to ensure the accuracy of the natural frequencies collected, four measure points are arranged.

The test results and simulation results are shown in Table 6, and the deviation is calculated. It can be seen from Table 6 that the difference of the first ten-order frequencies between the simulation results and the experimental results is small and the errors are less than 10% (except the third and fourth orders). The reason for the errors is that the actual boundary conditions and the fixed support of the steel foundation are slightly different, and the vibration modes of the 3rd and 4th orders are horizontal torsion. In addition, the omitted holes and actual chamfering in simulation will also bring fractional error. The comparison results imply that the modal analysis method is correct.

## 5. Thermal-Vibration Joint Test and Result Analysis

*5.1. Thermal-Vibration Joint Test System.* In order to complete the experiment at a high temperature, a thermal-vibration joint test system is developed by our team [33]. The structural block diagram of the system is shown in Figure 16. This system consists of two parts. One part is the thermal environment simulation test system to create a high-temperature environment. In this part, the temperature of the

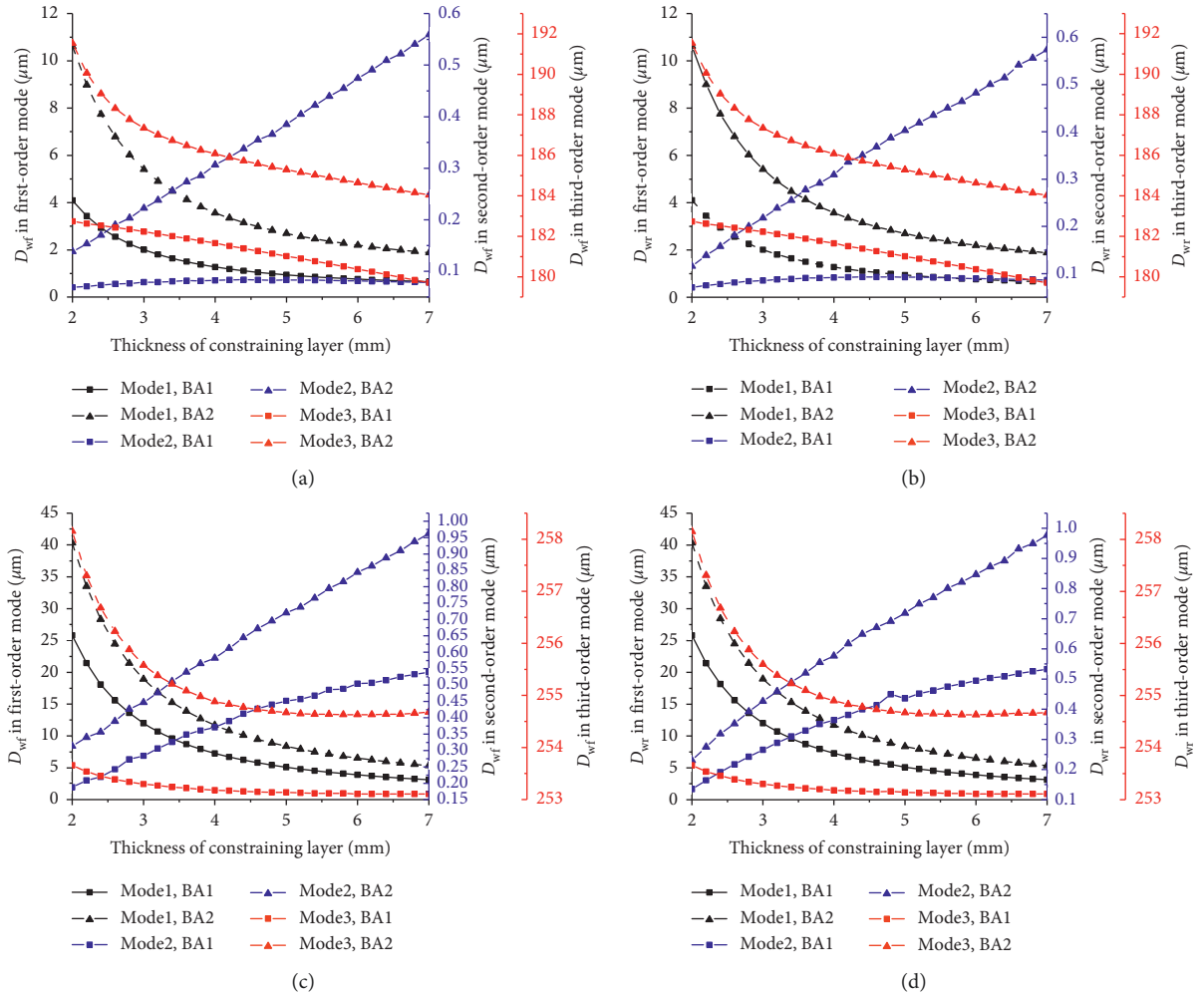


Figure 13: Displacement deviation between foundation and restraint layers in the position of the web plate. (a) Position I, upper constraining layer. (b) Position I, lower constraining layer. (c) Position II, upper constraining layer. (d) Position II, lower constraining layer.

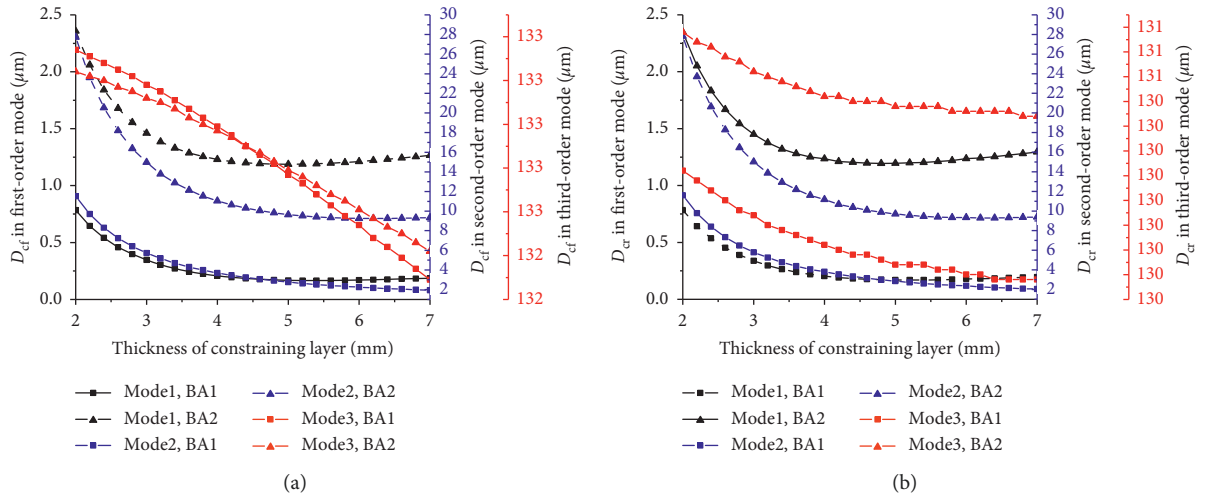


Figure 14: Continued.

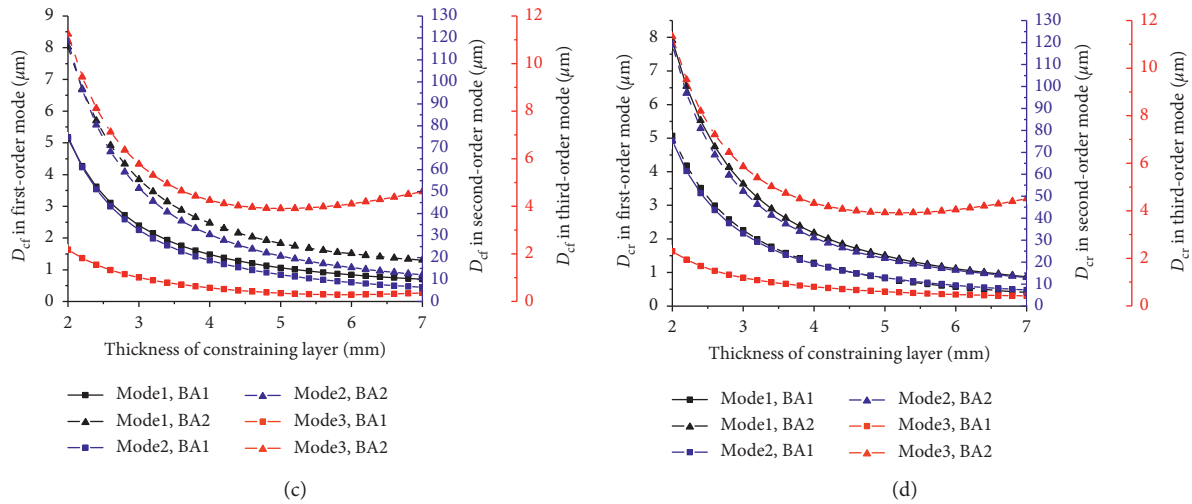


Figure 14: Displacement deviation between foundation and restraint layers in the position of the connection plate. (a) Position I, upper constraining layer. (b) Position I, lower constraining layer. (c) Position II, upper constraining layer. (d) Position II, lower constraining layer.

Table 5: Thickness of the constraining layer (unit: mm).

| Position | Face plate | | Bracket | | Web plate | | Connection plate | |
|---|---|---|---|---|---|---|---|---|
| | I | II | I | II | I | II | I | II |
| Upper constraining layer | 2 | 2 | 7 | 2 | 2 | 2 | 2 | 2 |
| Lower constraining layer | 2 | 2 | 7 | 2 | 2 | 2 | 2 | 2 |

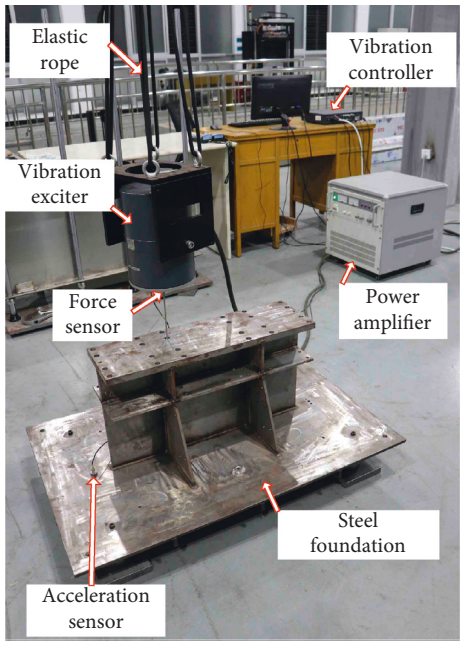


Figure 15: Test modal device.

foundation is controlled by a self-developed temperature control system based on LabVIEW®. The other is the vibration excitation and acquisition system. It is used to achieve excitation of the foundation at high temperature and the collection of corresponding test signals.

Table 6: Natural frequencies and vibration modes of test and simulation.

| Number | Vibration mode | Frequency (Hz) | | Error (%) |
|---|---|---|---|---|
| | | Simulation | Test | |
| 1 | Bending | 55.8 | 56.3 | 0.90 |
| 2 | Translation | 90.6 | 91.1 | 0.50 |
| 3 | Bending | 111.2 | 97 | 14.60 |
| 4 | Bending | 115.6 | 137.6 | 16.00 |
| 5 | Partial bending | 337.8 | 318.5 | 6 |
| 6 | Partial bending | 350.1 | 355.1 | 1.40 |
| 7 | Partial bending | 360.6 | 360.6 | 0 |
| 8 | Partial bending | 367.1 | 364.8 | 0.60 |
| 9 | Partial bending | 417.3 | 401.4 | 4.00 |
| 10 | Partial bending | 443.3 | 442.4 | 0.20 |

A temperature rise test was performed to evaluate the effect of temperature control. The target temperature was set as 100°C, 200°C, and 300°C, respectively. The temperature was kept for one hour at the target temperature to ensure that the foundation can be uniformly heated. Figure 17 shows the preset and control temperature on the foundation. It is noted that the temperature error is within ±5°C.

The thermal-vibration joint test system for the foundation is shown in Figure 18. The foundation is fixed on a rigid platform and is heated by the quartz lamp infrared heating arrays which are installed on the left and right sides of the foundation. Three aluminium silicate insulation boards are placed in the front/back/top of the foundation to provide heat insulation during heating. The electromagnetic

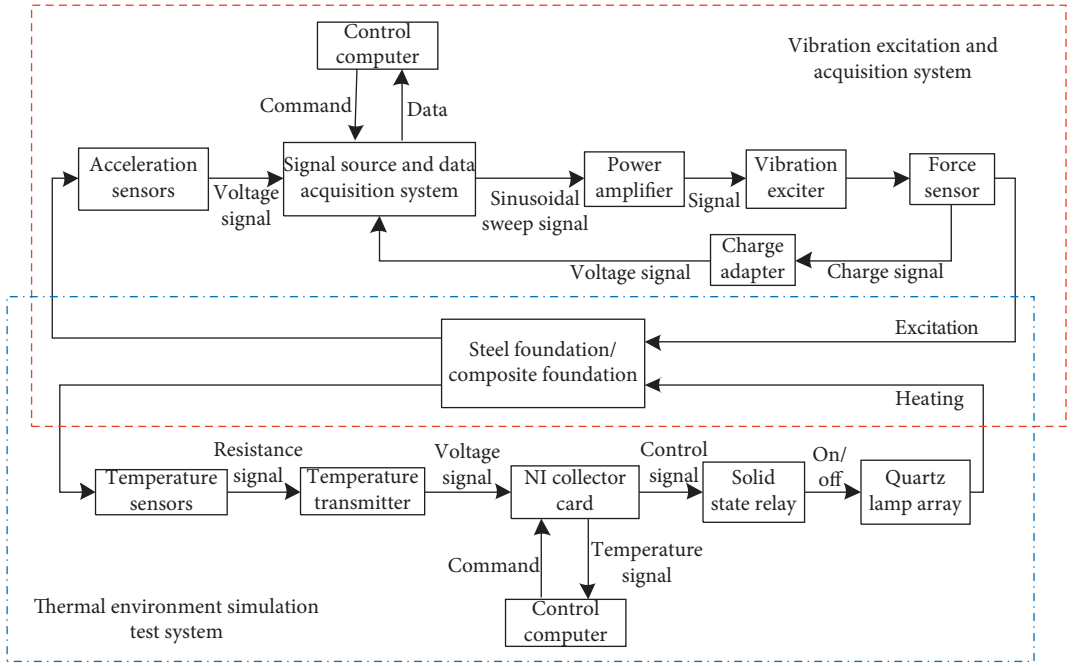


Figure 16: Block diagram of the thermal-vibration joint test system.

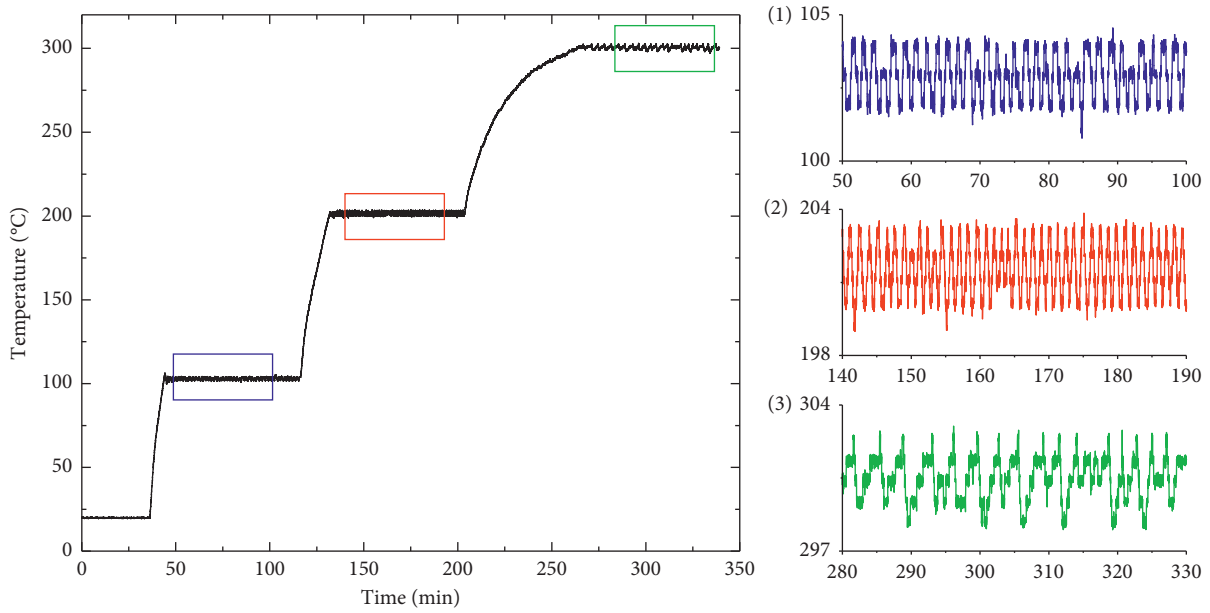


Figure 17: Preset and control temperature on the web plate.

exciter is suspended above the foundation by elastic ropes and is connected with the foundation by a ceramic connected pole. Different from the above modal test, four measuring points need to be arranged on the foundation to collect multidirectional signals, as shown in Figure 19. In order to save cost and avoid signal compensation, four common acceleration sensors are used. These sensors are installed outside the temperature field by four ceramic rods fixed at the measuring points. The upper limit of the operating temperature of the sensor is 150°C. In the actual experiment, the temperature of the upper end of the ceramic rod is about 70°C. Therefore, these sensors work within the permissible temperature.

*5.2. Test Results and Analysis of EMWM Composite Foundation.* The electromagnetic exciter sends sinusoidal sweep force to continuously excite the foundation. The parameters of the excitation signal are given in Table 7. The response of the foundation is detected by the use of four accelerometers. The excitation and response signals are recorded and processed using the signal source and data acquisition

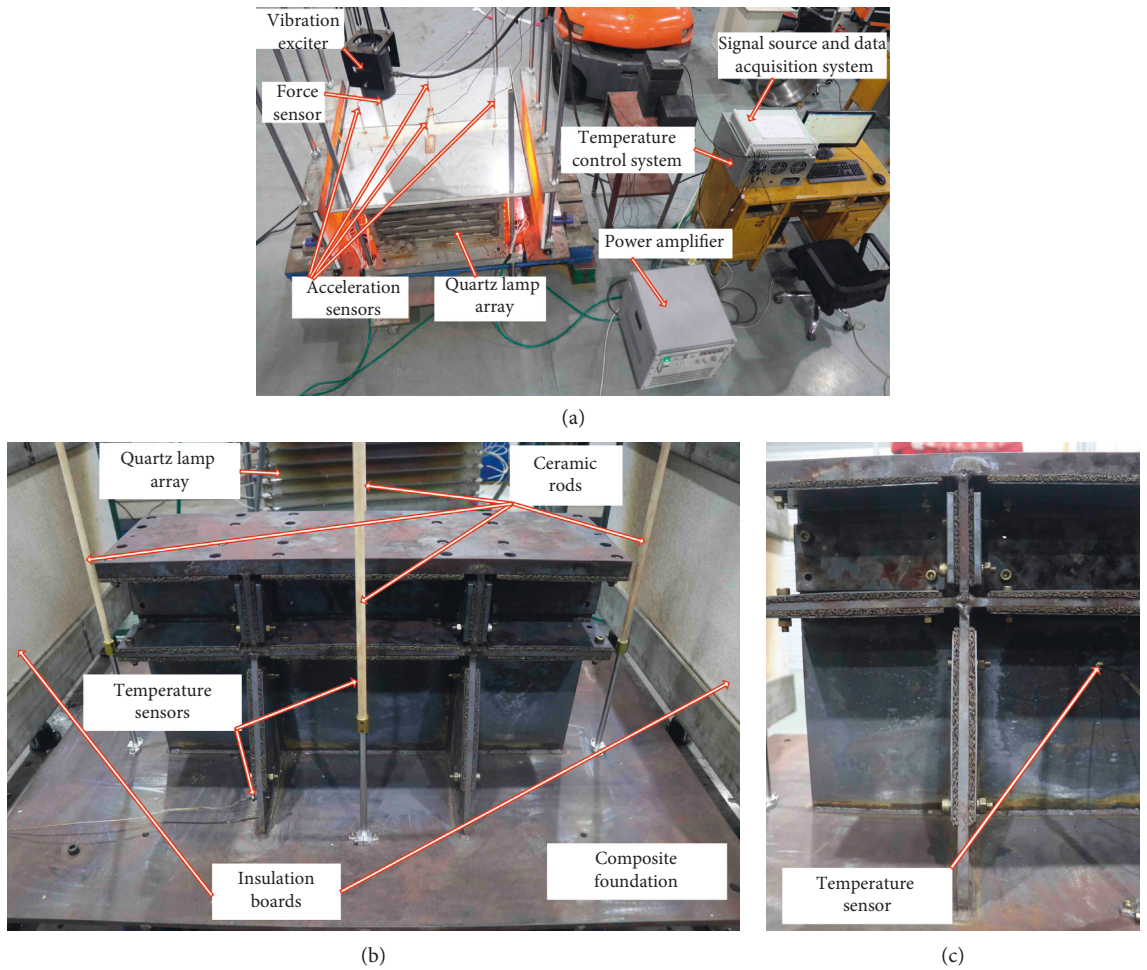


Figure 18: The thermal-vibration joint test system for foundation. (a) Test arrangement. (b) Composite foundation and temperature measuring point. (c) Temperature sensor.

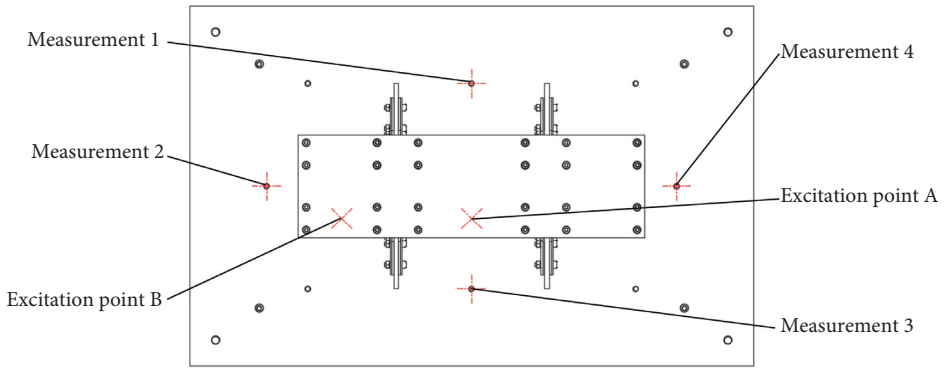


Figure 19: The arrangement of excitation point and measurement points.

Table 7: The parameters of the excitation signal.

| Parameters | Numerical value |
|---|---|
| Amplitude | 80 N |
| Waveform | Sine |
| Sweep mode | Logarithmic |
| Sweep range | 10~1000 Hz |

system in real time. The excitation points are A and B, as shown in Figure 19. The sweep rate is 1 oct/min. The ambient temperatures are 20°C and 300°C. According to equation (4), the average acceleration admittance $Z$ (the acceleration reference value is $10^{-6}$ m/s$^2$) of foundation is obtained. Insertion loss IL is calculated to evaluate the effect of insertion damping structure on the vibration reduction performance of the foundation.

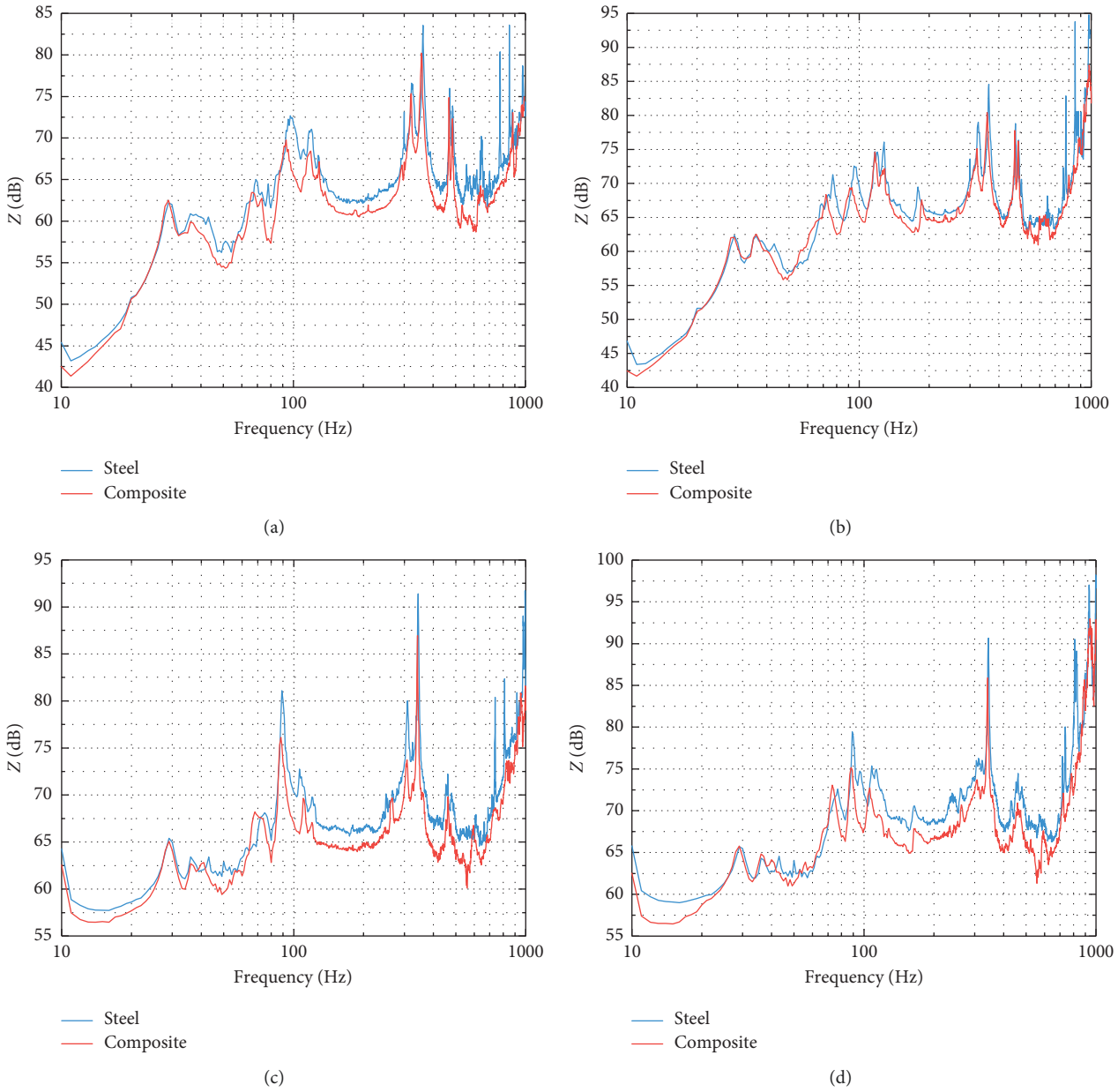


Figure 20: Acceleration admittance curve of steel foundation and composite foundation under different excitation points and temperatures. (a) 20°C, excitation point A; (b) 20°C, excitation point B; (c) 300°C, excitation point A; (d) 300°C, excitation point B.

$$Z = 20\lg\left(0.25\sum_{i=1}^{4}\frac{a_i}{F}\right) + 120, \tag{4}$$

$$\mathrm{IL} = Z_c - Z_0, \tag{5}$$

where $a_i$ is the acceleration value of the measuring point $i$, $F$ is the input force of the excitation point, $Z_c$ is the average acceleration admittance of the composite foundation, and $Z_0$ is the average acceleration admittance of the steel foundation.

The thermal-vibration joint test results of rigid foundation and composite foundation under room temperature and high temperature are shown in Figure 20.

Under room temperature, the peak value of IL at the first six modes is about 3.07 dB. The peak value of IL at the excitation point B is 0.7 dB larger than that at the excitation point A.

Under high temperature, $Z_c$ and $Z_0$ have a rise of 5–10 dB. The reason is that both foundations are thermally deformed, which is caused by the decrease of Young's modulus under high temperature. The average value of IL of the first six orders of the composite foundation is 4.11 dB. However, compared with the excitation point A, IL at excitation point B only changes 0.1 dB and the change is small. It means that, the influence of excitation points on the IL can be neglected in the first six modes.

As is shown in Figure 20, the composite foundation has good vibration damping performance in the mid-high-frequency range (500–1000 Hz), and the acceleration admittance drops by 7–15 dB regardless of temperature.

## 6. Conclusion

In this paper, the power flow was used as the evaluation index, and the energy transfer path of the foundation under single-point excitation was obtained. To reduce the vibration of the foundation, an EMWM composite foundation was designed. The reliability of the simulation and the damping performance of the composite foundation were validated by the modal validation and the thermal-vibration joint tests. The main conclusions, which can be drawn from the conducted simulations and tests, are as follows:

(1) The thickness of the horizontal constraining layer, such as the face plate and the connection plate, is negatively correlated with the displacement deviation between constraining layer and foundation. However, the relationship between the thickness of the constraining layer and the displacement deviation between constraining layer and foundation at the vertical plates, such as the brackets and the web plate, are complicated, and the change trend is changed according to the local stiffness and the various modes.

(2) When the ambient temperature is 20°C or 300°C, the composite foundation can effectively suppress the vibration in the analysis frequency band. The maximum vibration attenuation value can reach 15.37 dB. The attenuation value of the low-frequency band is slightly improved at a higher temperature than at room temperature. In addition, the insertion loss at room temperature changes slightly with the change of the excitation point, and the insertion loss does not change at high temperatures.

(3) The insertion damping structure with the entangled metallic wire material is presented. The damping performance of this structure is stable and effective at different temperatures.

## Data Availability

The data used to support the findings of this study are available from the corresponding author upon request.

## Conflicts of Interest

The authors declare no conflicts of interest.

## Acknowledgments

This study was supported by the National Natural Science Foundation of China (grant no. 51805086) and the Natural Science Foundation of Fujian Province, China (grant no. 2018J01763).

## References

[1] M. S. Yu, G. R. Huang, and T. X. Fu, "Development review on mechanical-noise control for submarine," *Journal of Ship Mechanic*, vol. 7, no. 4, pp. 110–120, 2003.

[2] X. L. Yao, Q. Y. Wang, F. Zhu, and F. Z. Pang, "Optimal design of vibration characteristics of ship pedestal with rigid vibration isolation mass," *Chinese Journal of Ship Research*, vol. 6, no. 05, pp. 23–27, 2011.

[3] Y. Shi, X. Zhu, and R. Q. Liu, "Analysis and experimental research on the role of quadrate steel beam in isolating vibration wave," *Shipbuilding of China*, vol. 45, no. 2, pp. 36–42, 2004.

[4] C. D. Che and D. S. Chen, "Analysis of the effect of blocking mass at corner interface of two plates at arbitrary angles on transmission of plane bending waves," *Chinese Journal of Acoustics*, vol. 32, no. 3, pp. 282–288, 2007.

[5] C. D. Che and D. S. Chen, "Attenuation effect of blocking mass attached at corner interface on transmission from plane longitudinal wave to bending wave," *Journal of Ship Mechanics*, vol. 15, no. 1, pp. 132–142, 2011.

[6] Q. Q. Xia and Z. J. Chen, "Design on impedance enhancement of ring stiffened cylindrical shell depressing low frequency line spectrum," *Journal of Harbin Engineering University*, vol. 34, no. 4, pp. 421–428, 2013.

[7] X. L. Yao, F. Ji, Z. H. Wang, and H. B. Zhou, "Numerical research on the full-band vibration and sound radiation of power cabin base with vibration isolation masses," *Ship & Boat*, vol. 4, pp. 34–42, 2010.

[8] X. W. Zhang, D. Q. Yang, and G. M. Wu, "A vibration and shock isolation synthesis design method for hybrid base," *Journal of Vibration & Shock*, vol. 35, no. 20, pp. 130–136, 2016.

[9] X. W. Zhang and D. Q. Yang, "A novel marine impact resistance and vibration isolation cellular base," *Journal of Vibration & Shock*, vol. 34, no. 10, pp. 40–45, 2015.

[10] B. H. Wu, X. W. Zhang, and D. Q. Yang, "Mechanical properties and application of the star-shaped cellular auxetic material," *Chinese Journal of Solid Mechanics*, vol. 39, no. 02, pp. 139–151, 2018.

[11] B. H. Wu, X. W. Zhang, and D. Q. Yang, "Real ship application analysis of vibration isolation base made by auxetic metamaterials," *Ship Engineering*, vol. 40, no. 02, pp. 56–62, 2018.

[12] H. X. Qing and D. Q. Yang, "Functional element topology optimal method of metamaterial design with arbitrary negative Poisson's ratio," *Acta Materiae Compositae Sinica*, vol. 35, no. 04, pp. 1014–1023, 2018.

[13] H. X. Qing, D. Q. Yang, and X. W. Zhang, "Vibration reduction of auxetic acoustic metamaterial mount," *Journal of Vibration Engineering*, vol. 30, no. 6, pp. 1012–1021, 2017.

[14] L. B. Liu, H. B. Wen, C. H. Wu, and T. Wang, "Application and experimental research on composite vibration reduction structure of ship pedestal," *Ship Science & Technology*, vol. 37, no. 10, pp. 47–51, 2015.

[15] M. R. Garrison, R. N. Miles, J. Q. Sun, and W. Bao, "Random response of a plate partially covered by a constrained layer damper," *Journal of Sound and Vibration*, vol. 172, no. 2, pp. 231–245, 1994.

[16] I. Merideno, J. Nieto, N. Gil-Negrete, J. G. Giménez Ortiz, A. Landaberea, and J. Iartza, "Influence of sandwich-type constrained layer damper design parameters on damping strength," *Shock and Vibration*, vol. 2016, Article ID 7846369, 14 pages, 2016.

[17] V. D'Alessandro, G. Petrone, F. Franco, and S. De Rosa, "A review of the vibroacoustics of sandwich panels: models and

experiments," *Journal of Sandwich Structures & Materials*, vol. 15, no. 5, pp. 541–582, 2013.

[18] D.-W. Wang and L. Ma, "Sound transmission through composite sandwich plate with pyramidal truss cores," *Composite Structures*, vol. 164, pp. 104–117, 2017.

[19] J. Lou, B. Wang, L. Ma, and L. Z. Wu, "Free vibration analysis of lattice sandwich beams under several typical boundary conditions," *Acta Mechanica Solida Sinica*, vol. 26, no. 5, pp. 458–467, 2013.

[20] J. Yang, J. Xiong, L. Ma, B. Wang, G. Zhang, and L. Wu, "Vibration and damping characteristics of hybrid carbon fiber composite pyramidal truss sandwich panels with viscoelastic layers," *Composite Structures*, vol. 106, no. 12, pp. 570–580, 2013.

[21] S. Assaf and M. Guerich, "Numerical prediction of noise transmission loss through viscoelastically damped sandwich plates," *Journal of Sandwich Structures & Materials*, vol. 10, no. 5, pp. 359–384, 2008.

[22] K. Wu, H. Bai, X. Xue, T. Li, and M. Li, "Energy dissipation characteristics and dynamic modeling of the coated damping structure for metal rubber of bellows," *Metals*, vol. 8, no. 7, p. 562, 2018.

[23] D. Y. Zhang, Y. Xia, Q. C. Zhang, Y. H. Ma, and J. Hong, "Researches on metal rubber mechanics properties in retrospect and prospect," *Journal of Aerospace Power*, vol. 33, no. 06, pp. 1432–1445, 2018.

[24] A. M. Zhizhkin, G. V. Lazutkin, D. P. Davydov, and T. D. Volkova, "Influence of porous material MR structure on its flow characteristics," *Materials Science and Engineering*, vol. 302, Article ID 012074, 2018.

[25] D. Rodney, B. Gadot, O. R. Martinez, S. R. Du Roscoat, and L. Orgéas, "Reversible dilatancy in entangled single-wire materials," *Nature Materials*, vol. 15, no. 1, pp. 72–77, 2016.

[26] H. Yu, X. Sun, J. Xu, and S. Zhang, "Transition sets analysis based parametrical design of nonlinear metal rubber isolator," *International Journal of Non-linear Mechanics*, vol. 96, pp. 93–105, 2017.

[27] T. A. Chirathadam and L. S. Andrés, "Measurements of rotordynamic response and temperatures in a rotor supported on metal mesh foil bearings," *Journal of Engineering for Gas Turbines and Power*, vol. 135, no. 12, Article ID 122507, 2013.

[28] H. B. Bai, C. H. Lu, and F. L. Cao, *Metal Rubber Material and Engineering Application*, Science Press, Beijing, China, 1st edition, 2014.

[29] J. F. Hou, H. B. Bai, and D. W. Li, "Damping capacity measurement of elastic porous wire-mesh material in wide temperature range," *Journal of Materials Processing Technology*, vol. 206, no. 1–3, pp. 412–418, 2008.

[30] Y. Y. Wang, H. B. Bai, and Y. F. Liu, "Micro characteristic study of the compressive performance of metal rubber material," *Mechanical Science & Technology for Aerospace Engineering*, vol. 30, no. 3, pp. 404–407, 2011.

[31] L. Gavric and G. Pavic, "A finite element method for computation of structural intensity by the normal mode approach," *Journal of Sound and Vibration*, vol. 164, no. 1, pp. 29–43, 1993.

[32] G. Petrone, M. De Vendittis, S. De Rosa, and F. Franco, "Numerical and experimental investigations on structural intensity in plates," *Composite Structures*, vol. 140, pp. 94–105, 2016.

[33] Z. Ding, H. Bai, Y. Wu, Y. Zhu, and Y. Shao, "Experimental investigation of thermal modal characteristics for a ship's foundation under 300°C," *Shock and Vibration*, vol. 2019, Article ID 2714930, 11 pages, 2019.